

<https://doi.org/10.1038/s41528-025-00456-x>

# High resolution reverse-offset printed wearable laminated textile capacitive sensor for continuous monitoring of atopic dermatitis



Huanghao Dai<sup>1</sup> ✉, Alexandar R. Todorov<sup>1</sup>, Sheng Yong<sup>1</sup>, Russel Torah<sup>1</sup>, Michael Ardern-Jones<sup>2</sup> & Steve Beeby<sup>1</sup> ✉

Reverse-offset printing (ROP) enables microscale patterning on flexible substrates, making it ideal for fabricating interdigital capacitive (IDC) sensors for atopic dermatitis (AD) monitoring. AD, characterized by skin dryness and inflammation, demands precise hydration tracking. Tailoring IDC electrode gaps to 50  $\mu\text{m}$  concentrates the electric field within the stratum corneum (SC), enhancing sensitivity beyond the capabilities of traditional screen printing. Finite element modelling and ROP were employed to assess the impact of electrode geometry and encapsulation thickness on sensor performance. Findings indicate that 50  $\mu\text{m}$  electrodes with encapsulation layers under 10  $\mu\text{m}$  maintain high sensitivity and consistent operation. A clinical case study demonstrated the 50  $\mu\text{m}$  sensor's ability to distinguish lesional from non-lesional skin. These results inform the optimization of encapsulation–performance balance and advance the design of wearable, high-resolution IDC sensors for continuous skin hydration monitoring in personalized dermatological care.

Recent advances in skin sensing technology have led to increasing applications in health monitoring and evaluating environmental interactions<sup>1–4</sup>. The ability to measure parameters such as hydration<sup>5,6</sup>, temperature<sup>7,8</sup>, and pH<sup>9,10</sup> directly from the skin offers valuable insights into physiological conditions and external influences, enhancing diagnostics, and enabling personalized healthcare<sup>11</sup>. Atopic dermatitis (AD), commonly referred to as atopic eczema, is the most prevalent inflammatory skin condition worldwide, with prevalence rates ranging from 15–30% in children and 2–10% in adults<sup>12,13</sup>. This chronic and relapsing disorder is characterized by recurring inflammation and dryness of the skin, potentially leading to cuts and lesions which can then manifest into significant infections, and even become life-threatening in extreme cases<sup>14</sup>. Damage to the stratum corneum (SC), the outermost skin layer, makes it prone to external factors such as allergens and bacteria and causes excessive water loss from the skin<sup>15,16</sup>, as Fig. 1a shows. To monitor the severity of AD, various textile-based sensors have been demonstrated as shown in Table 1. They primarily utilize two methods: skin hydration level monitoring and scratching movement detection. Hydration sensors assess the moisture content of the SC to evaluate skin barrier function, while motion sensors track scratching behavior, a key indicator of itch severity. Among these, interdigitated capacitive (IDC) sensors are

particularly promising due to their high sensitivity to hydration changes and ease of fabrication through printing techniques such as screen printing. This makes IDC sensors an ideal choice for scalable, low-cost, and wearable solutions for continuous AD monitoring.

The structure of IDC sensor comprises two individual planar electrodes with an interdigitated comb arrangement that form multiple parallel plate capacitors, and the basic structure is shown in Fig. 1b. IDC sensors have emerged as a promising solution in wearable applications, such as human motion detection<sup>17,18</sup> and touch sensing<sup>19</sup>, due to their high sensitivity, ease of fabrication, and suitability for integration into electronic textiles (e-textiles)<sup>20</sup>. Substances applied to the surface of, or materials placed in contact with, the IDC will also alter the capacitance depending upon the dielectric properties of the applied material. Figure 1c shows the IDC sensor placed on the skin and connected to an impedance analyzer, enabling real-time monitoring of skin capacitance changes associated with AD. When placed in contact with the skin, variations in capacitance can be measured, reflecting changes in the skin's properties, such as the relative permittivity of the SC layer, which correlates directly with hydration levels<sup>21,22</sup>. Previous studies have demonstrated the efficacy of IDC sensors. For instance, Kim et al. showcased the use of IDC sensors for real-time monitoring of skin

<sup>1</sup>Centre for Flexible Electronics and E-Textiles (C-FLEET), University of Southampton, Southampton, UK. <sup>2</sup>School of Clinical Experimental Sciences, Faculty of Medicine, University of Southampton, Southampton, UK. ✉e-mail: [hd2m19@soton.ac.uk](mailto:hd2m19@soton.ac.uk); [spb@ecs.soton.ac.uk](mailto:spb@ecs.soton.ac.uk)

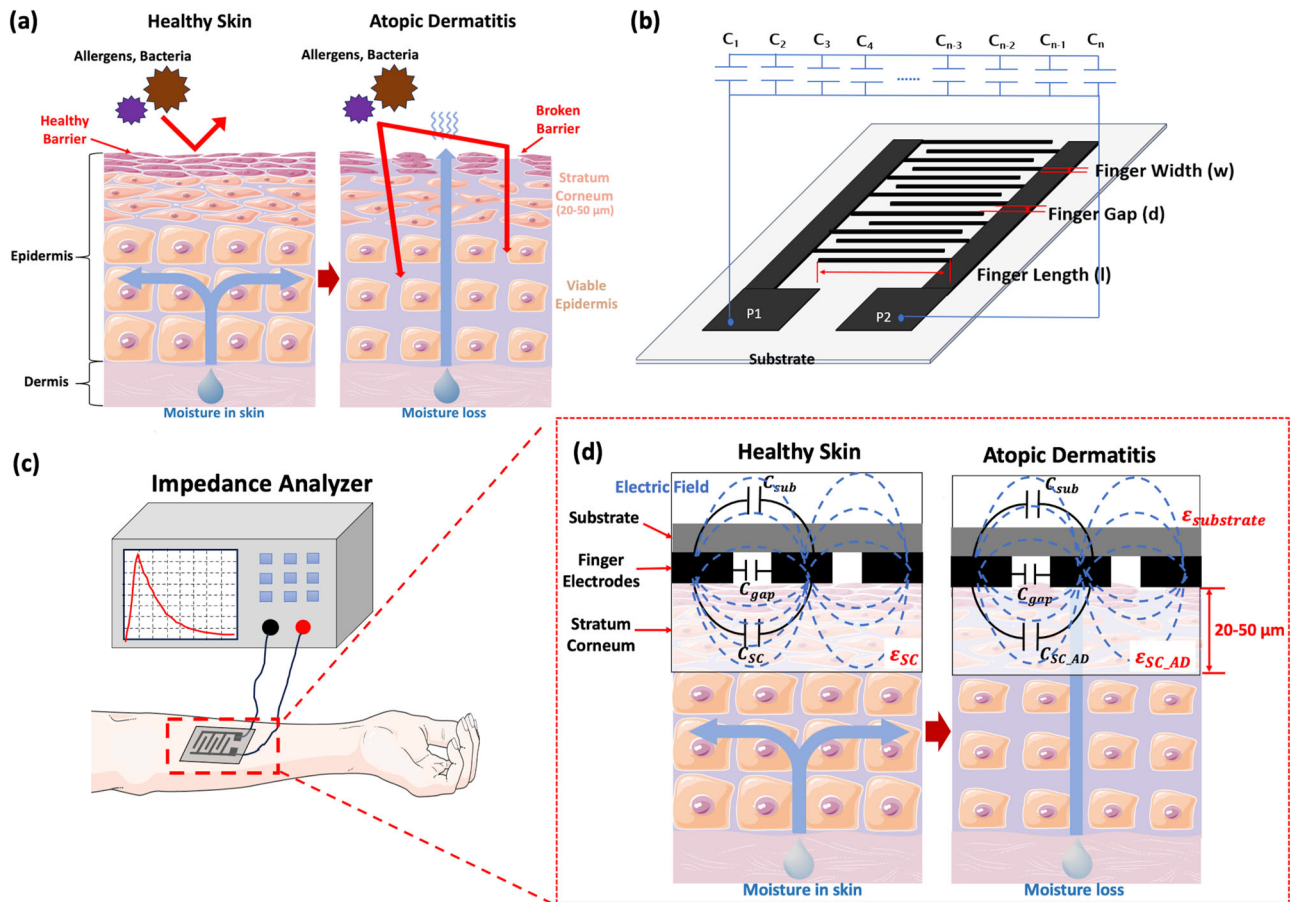


**Fig. 1 | Background information.** **a** Comparison of cellular structure in healthy skin versus skin with AD. **b** Schematic diagram of IDC sensor’s working mechanism. **c** Schematic diagram of the IDC sensor attached to the skin and connected to an impedance analyzer for continuous monitoring of AD. **d** Schematic diagram of the

generated electric field lines distribution for the IDC sensor on healthy skin (left) and AD-affected skin (right). (Images reproduced from Servier Medical Art by Servier, licensed under CC BY 3.0).

hydration, demonstrating their ability to detect changes in skin hydration with a sensitivity of less than 0.01 pF per percentage change in skin moisture providing a reliable and non-invasive method for skin analysis<sup>23</sup>. Similarly, Sapsanis et al. highlighted the flexibility and high sensitivity of IDC sensors. Their research demonstrated a flexible Nafion-coated IDC humidity sensor on a flexible substrate, achieving high sensitivity with linear behavior above 65% RH (relative humidity) and slightly non-linear behavior below, while maintaining performance under bending<sup>24</sup>. The sensitivity of the IDC sensors is closely related to the electric field depth generated by the interdigitated electrodes which should be designed to match the application parameters<sup>25</sup>. In the case of monitoring AD, the IDC must be designed such that the electric field is concentrated within the SC layer, which has a thickness of 20–50 μm, as shown in Fig. 1d. An IDC with more densely packed electrodes (smaller finger gap and finger width) will generate a higher electric field intensity near the surface, but with a shallower penetration and thus providing greater sensitivity to any dielectric property changes in the skin. Huang et al. investigated the design of IDC sensors and analyzed the effect of electrode dimensions, such as width and thickness, on sensitivity and penetration depth, showing the need for a balance between them for optimal sensor performance<sup>26</sup>. Adjusting the IDC design and accommodating the presence of any encapsulation layer can effectively modulate the field depth and enhance sensor performance<sup>27,28</sup>. This was explored by Kim et al. who identified that to achieve the desired electric field depth within the SC layer, the combined electrode finger spacing and finger width should be around 30–100 μm<sup>29</sup>.

Realizing such precise electrode structures requires advanced fabrication techniques. Among these, printing techniques offer significant benefits

because they enable the efficient production of solution-processed electronics with multilayer architectures—ensuring both high resolution and mechanical flexibility, which are essential for wearable applications<sup>30,31</sup>. They have been widely used to realise a wide range of devices including solar cells<sup>32</sup>, metal oxide transistors<sup>33</sup> and organic electrochemical transistors<sup>34</sup>. While common printing methods like inkjet and screen printing are widely used to manufacture flexible and wearable devices, their resolution is often constrained by factors such as the nozzle size or mesh dimensions. Ordinary inkjet printing typically achieves feature sizes of approximately 100–500 μm, while conventional screen printing with standard mesh screen generally achieves 200–1000 μm. Previous examples of printed IDC sensor research demonstrated an inkjet-printed single-port IDC sensor with a finger width and spacing of 0.5 mm<sup>35</sup> and a screen-printed flexible IDC sensor with finger widths and spacings of 0.5 mm, 0.8 mm, and 1.2 mm<sup>36</sup>. These printing methods cannot typically achieve the fine resolutions required to maximise the performance of the IDC sensor in the AD monitoring application. To overcome these challenges, reverse offset printing (ROP) offers a relatively new solution by enabling high-resolution printed patterns with minimum feature sizes often reaching down to the micron range, making it ideal for advanced IDC sensor fabrication. The benefits of reverse offset printing also include high throughput, cost-effectiveness, and compatibility with a wide range of inks. Choi et al. demonstrated that reverse-offset printing can achieve ultra-fine patterns with line widths of 10 μm, which is critical for applications such as transparent touch screen sensors where the small minimum feature size provides an ultrafine conductive pattern with high transmittance<sup>37</sup>. Furthermore, roll-to-roll printing is a scalable and efficient manufacturing process, ideal for the cost-effective

**Table 1 | Summary of textile-based sensors for atopic dermatitis (AD) monitoring**

Monitoring Method	Sensor Type	Sensing Mechanism	Fabrication Process and Materials	Resolution	Patient Testing	Comments
Skin Hydration Monitoring	Reverse-offset printed IDC sensors (this research)	Capacitance changes correlate with SC hydration (dielectric shifts in AD lesions).	Reverse-offset printed Ag electrodes on TPU substrate laminated on the textile with EVOH encapsulation.	Electrode width/spacing 50 $\mu\text{m}$ .	Yes	High-resolution hydration level tracking; clinical validation; optimized encapsulation for wearable flexibility and sensitivity.
	Impedance-based textile sensor <sup>5</sup>	Impedance decreases with hydration, targeting the SC and epidermis.	Screen-printed Ag electrodes on cotton with TPU encapsulation.	Electrode width: 5 mm; gap: 1 mm.	Yes	Validated against a commercial sensor (KAKUSAN SK-IV); low resolution (5 mm) reduces SC specificity; deep penetration (> 5 mm) affects accuracy.
Scratching Detection	Wireless skin hydration sensor (SHS) <sup>6</sup>	Measures skin water content (0–1 mm depth) via transient thermal response; integrates with NFC smartphones.	Laser-cut and micro-soldered flexible PCB with dual-coil antennas, silicone adhesive, and fiberglass reinforcement.	~60 $\mu\text{m}$ spacing between heater and sensor	Yes	Measures deeper layers (> 100 $\mu\text{m}$ ), reducing SC specificity; complex fabrication process.
	Interdigitated capacitive (IDC) sensor <sup>16</sup>	Measures changes in capacitance due to hydration variations.	Screen-printed silver-loaded polymer on textile armband.	Electrode width/ gap 200 $\mu\text{m}$	No	Good correlation to Comeometer™, but there is no AD patient validation; low resolution limits sensitivity.
Itch monitoring wristband <sup>23</sup>	Sensorised glove <sup>51</sup>	Detects finger bending via microtubular strain sensors and arm motion; Machine learning classifies scratching (83–99% accuracy).	Custom assembly on off-the-shelf glove, microtubular sensors (silicone + liquid metal), 3D-printed control unit.	Microchannel diameter: 0.16 mm	Yes	Detects scratching movements with 83%–99% classification accuracy. However, because it cannot distinguish non-scratching actions, the sensitivity varies with types of motion.
	Itch monitoring wristband <sup>23</sup>	Accelerometer detects wrist motion; algorithm classifies scratching (74–99% accuracy).	Cotton wristband with integrated accelerometer.	Device dimensions: 300 mm x 30 mm	Yes	User-friendly design but cannot differentiate scratching from high-frequency motions (e.g., waving).

mass production of large-area electronic devices due to its high throughput and continuous operation<sup>38</sup>.

Existing wearable sensors for AD monitoring, as summarized in Table 1, face limitations in resolution, specificity to the SC, or clinical validation. To address these gaps, this work introduces a ROP printed IDC sensor on fabrics tailored for high-resolution SC hydration monitoring. Leveraging ROP fabrication, the sensor achieves 50  $\mu\text{m}$  electrode spacing—critical for targeting the SC layer (20–50  $\mu\text{m}$ )—while maintaining compatibility with textile integration for wearability. The paper details the materials, cliché fabrication, and sensor fabrication processes and through COMSOL simulations and experimental results, investigates the impact of feature size and encapsulation layer thickness on sensor performance. The resulting sensor demonstrates enhanced accuracy in distinguishing AD lesions from healthy skin, validated through clinical testing. This approach bridges the gap between high-resolution diagnostics and practical wearable design, offering a scalable solution for personalized dermatological care.

## Results

### COMSOL Multiphysics Simulation

The simulation of the IDC sensor consists of two finite element (FE) models: a non-encapsulated IDC sensor model and an IDC sensor with an encapsulation layer covering the electrodes. The non-encapsulated IDC sensor model was first used to explore sensitivity versus printed feature size and the IDC sensor with the encapsulation layer model was then used to evaluate the influence of the encapsulant.

### IDC Sensor Sensitivity vs. Feature Sizes

To simulate the effect of IDC finger width and gap on the sensitivity to skin hydration level, an IDC sensor was designed on a flexible thermoplastic polyurethane (TPU) substrate that would subsequently be laminated on to a textile shown in Fig. 2a. A 3-dimensional (3D) model was developed in COMSOL Multiphysics 6.1 with a stratum corneum (SC) skin layer with thickness of 50  $\mu\text{m}$  positioned above the IDC sensing fingers as shown in Fig. 2b. IDC's with finger widths and gaps of 50  $\mu\text{m}$ , 100  $\mu\text{m}$ , and 200  $\mu\text{m}$  (referred to as G50W50, G100W100, and G200W200, respectively) were simulated where the 200  $\mu\text{m}$  case represents a previous screen-printed IDC sensor<sup>16</sup> and the 50  $\mu\text{m}$  represents an IDC that can be reliably printed with a bespoke ROP printer<sup>39</sup>. The sensing area was fixed at 0.7 mm x 3 mm and therefore 32, 16, and 8 finger pairs are realised for the G50W50, G100W100, and G200W200 IDC designs respectively. The hydration levels were modified by adjusting the relative permittivity of the SC layer between 500 (representing extremely dry skin), 1100 (representing normal skin) and 2100 (representing extremely hydrated skin)<sup>40</sup>. The specific parameters of the IDC sensor model are given in the Method section. The total sensor capacitance within the SC layer in contact with electrode fingers was determined using COMSOL Multiphysics' Maxwell capacitance calculation. For all models, a potential of 1 V<sub>ac</sub>, the IDC sensor's operating power, at 10 kHz, a commonly optimized working frequency, was applied between the two electrodes. The simulated results are shown in Fig. 2c. The G50W50 sensor exhibits the highest sensitivity to changes in the relative permittivity of the SC layer whilst the G200W200 design exhibits the lowest sensitivity, confirming the importance of concentrating the electric field with the SC layer.

### Encapsulation Layer Thickness Effects on IDC Sensor Performance

The printed electrodes are exposed on the surface and, given a printed feature thickness of around 5–10  $\mu\text{m}$ , are vulnerable to physical damage and are sensitive to external factors such as moisture and dust. Therefore, it is desirable to apply an encapsulation layer on top of the IDC sensing area to protect the IDC sensor and ensure accurate operation in real-world environments over its intended lifespan. The sensing mechanism of the IDC sensor relies on the generated electric field being introduced within the SC layer, but the presence of an encapsulation layer with a given dielectric constant will affect the electric field and its penetration depth. Therefore, the

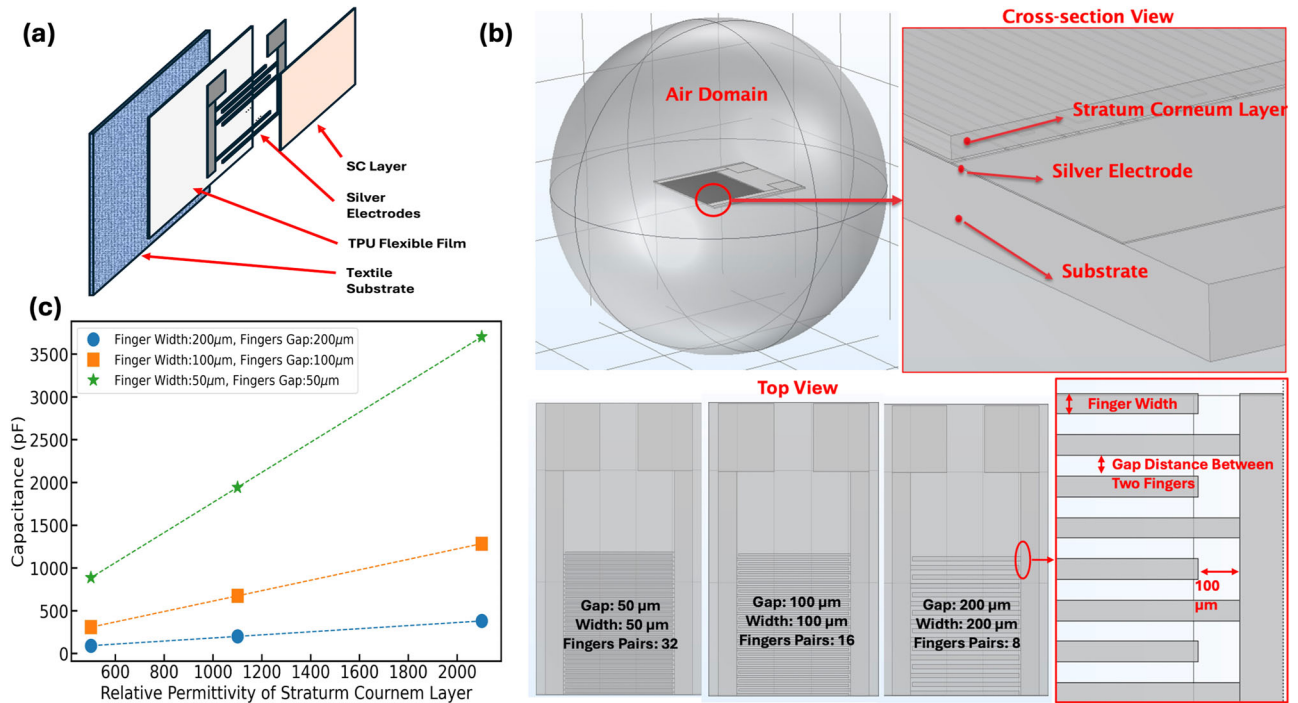


**Fig. 2 | IDC sensor model built using COMSOL Multiphysics 6.1.** **a** Schematic exploded diagram of the IDC sensor structure. **b** G50W50, G100W100, and G200W200 IDC sensor 3D models built separately in COMSOL Multiphysics with

isometric and top view of the sensor models. **c** Simulation results of the effect of varying SC layer relative permittivity on the capacitance of sensors with varying finger widths and gaps.

influence of the encapsulation layer on the electric field has been simulated using the IDC sensor design shown in Fig. 3(a) and a 3D model of the G50W50 sensor is shown in Fig. 3(b).

Three potential encapsulants were investigated: ethylene vinyl alcohol (EVOH), polymethyl methacrylate (PMMA), and polydimethylsiloxane (PDMS). These are widely used in encapsulation applications due to their excellent barrier properties, mechanical stability, and flexibility<sup>41–44</sup>. The encapsulating materials were simulated with thicknesses of 2 μm, 5 μm, 10 μm, and 15 μm and the resulting change in capacitance between hydrated skin and dry skin cases is presented in Fig. 3 (c) where the capacitance difference represents device sensitivity. The presence of the encapsulating layer significantly reduces sensitivity compared with the non-encapsulated G50W50 sensor which has a capacitance difference of 2815.9 pF between the hydrated and dry skin cases. The thickness of the three encapsulation layers also has an impact on the capacitance change with the thicker layers preventing the IDC sensor from detecting any change in the SC. Among the three materials, the EVOH layer has the least effect on device sensitivity and was therefore evaluated further in practical tests. Figure 3 (d) shows the capacitance as a function of the relative permittivity of the SC layer, for various thicknesses of the EVOH encapsulation layer, which confirms that the thinner EVOH layers (2 μm and 5 μm) are preferred to maintain sufficient sensitivity. Further COMSOL simulations at physiologically relevant SC layer thicknesses of 25 μm and 50 μm (Supporting Information Section S1, Table S1) demonstrate that these sensitivity trends—and the optimal 2 μm encapsulation—remain unchanged, validating the use of a 50 μm SC layer model in the main text. To analyze the electric field distribution around the IDC sensor, a 2-dimensional (2D) model of the ROP G50W50 sensor was built in COMSOL Multiphysics 6.1 as shown in Fig. 4(a). Figure 4(b) shows the generated electric field for the non-encapsulated IDC sensor which is concentrated around the SC layer and matches the desired distribution shown in Fig. 1(d). EVOH encapsulation layers with thicknesses of 2 μm, 5 μm, 10 μm, and 15 μm were added between the IDC and the SC layer and the resulting electric field distributions are shown in Fig. 4(c), (d), (e) and (f). The results show that the encapsulating layer reduces the penetration depth within the SC and thicker EVOH layers should be avoided. Table

2 gives the simulated electric field strength at four points (A, B, C, D as shown in Fig. 4(b)) located over the centre of each finger 3 μm into the SC layer. These results quantify the influence of EVOH thickness with the electric field being visibly concentrated in the encapsulation layer, reducing the field in the SC layer and leading to the reduced sensitivity. In addition to the 2-D planar simulations, we performed a 2-D curved-surface analysis (bending radius = 222.8 μm) to validate the model under realistic forearm curvature. The results (Supporting Information Section S2, Table S2) show < 10% deviation in field strength and identical sensitivity trends, justifying the use of planar simulations for device design on curved skin.

### Reverse-Offset Printed (ROP) Interdigital Capacitive (IDC) Sensor

The sensors were fabricated using a bespoke ROP printer<sup>39</sup> (described in the Method section) following three main steps as illustrated in Fig. 5(a). Step 1 is the coating process where functional inks are applied to the PDMS covered roller via a doctor-blade coater to form a flat and uniform ink film as shown in Fig. 5(b). Step 2 is the removal process where the roller moves across the stencil or etched silicon plate (known as a cliché plate) which has high surface energy and deep intaglios as the SEM picture in Fig. 5(c) shows. The raised areas of the cliché form a negative image of the desired pattern and ink is transferred from the PDMS blanket to the cliché (Fig. 5(d)). Step 3 is the printing process where the ink remaining on the blanket (see Fig. 5(e)) is transferred to the substrate as the roller rolls across its surface as shown in Fig. 5(f). The roller speed and contact pressure must be controlled to successfully print the pattern on the target substrate. The silicon cliché with the IDC geometry etched into its surface was fabricated using standard photolithography and deep reactive ion etching (DRIE). TPU was selected as the printable substrate because it combines the high flexibility (easily bending around a forearm) and thermal stability (> 150 °C) required for depositing fine conductive patterns via ROP, while still providing enough mechanical robustness for skin-contact applications. While TPU does not stretch in all directions like elastomers, the small dimensions of the developed IDC sensors require only simple bending—not full conformity—to maintain epidermal contact. To enhance wearability, the printed TPU layer is

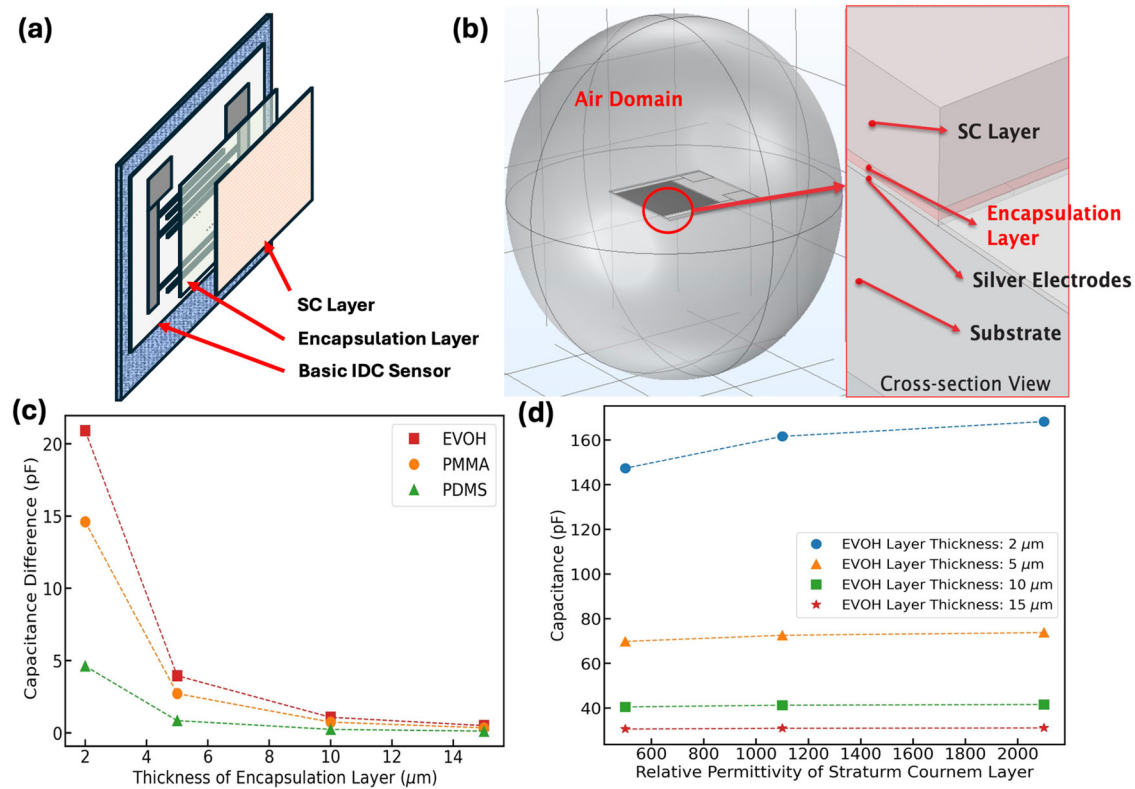


**Fig. 3 | Simulation of encapsulation layer thickness effects on IDC sensor performance in COMSOL Multiphysics 6.1. a** Schematic exploded diagram of the encapsulated IDC sensor structure. **b** 3D model of the encapsulated IDC sensor with the finger width and gap of 50  $\mu\text{m}$  built in COMSOL Multiphysics with cross-section

and top view of the sensor model. **c** IDC sensor capacitance difference between contacting with hydrated and dry skin vs. thickness of encapsulation layer for EVOH, PMMA, and PDMS. **d** Impact of EVOH encapsulation layer thickness on capacitance change of IDC sensor due to varying skin conditions.

laminated onto a soft textile, combining precise patterning with textile-level flexibility and comfort. The three IDC sensor geometries were successfully printed on the TPU films and SEM photos of electrode fingers of the G50W50 sensor are shown in Fig. 5(g), which shows well-defined silver lines with the desired feature sizes.

Each IDC sensor was laminated on to an arm band with a strap as shown in Fig. 6(a) which enables straightforward attachment to a human subject and provided repeatable results. The sensors were characterised in free air and in contact with human skin, located on the arm as shown in Fig. 6(b) with dry and hydrated skin. The IDC capacitance was measured versus frequency for the G50W50, G100W100, and G200W200 sensors without an encapsulation layer and results are shown separately in Fig. 6(c), (d) and (e). In all cases, the free space control capacitance remains constant, and each sensor responds to contact with the dry and hydrated skin. In each case, the hydrated skin exhibits higher capacitance (blue line) due to its higher dielectric constant, whilst the dry skin (orange line) shows consistently lower capacitance values. The error bars illustrate that the measurements are consistent and repeatable. The sensitivity of the three sensors is compared in Fig. 6(f) which indicates the G50W50 sensor consistently shows the highest capacitance difference between the dry and hydrated states across all frequencies. As the finger gap and width increase, the capacitance difference decreases illustrating the benefits of the higher-resolution devices achieved by ROP.

To validate the COMSOL simulation of the encapsulation layer materials and thicknesses on IDC sensor performance, various encapsulation layers were added to previously characterised IDC sensors. The EVOH, PMMA and PDMS films were spin coated on to the G50W50, G100W100, and G200W200 sensors as shown in Fig. 7(a) with the SEM cross-section of the EVOH encapsulated sensor shown in Fig. 7(b). The capacitance difference measured from hydrated and dry skin using the G50W50 IDC sensor encapsulated with the three different materials is

shown in Fig. 7(c). As expected, all encapsulation materials reduce the sensitivity and the EVOH layer has the least effect followed by the PMMA and PDMS respectively which matches the simulated results shown in Fig. 3(c). The EVOH layer was initially spin-coated at 1500 rpm onto the G50W50, G100W100, and G200W200 IDC sensors achieving an EVOH encapsulation layer  $15 \pm 0.05 \mu\text{m}$  thick. To compare the performance of these sensors with and without the EVOH encapsulation layer, the capacitance measured from dry and hydrated skin before and after coating the encapsulation layer on the otherwise same device is shown in Fig. 7(d), (e) and (f). Without encapsulation, there is a large initial difference in capacitance between hydrated skin (blue line) and dry skin contact (orange line), which decreases sharply with frequency. With encapsulation, the capacitance difference between hydrated skin (green line) and dry skin (red line) is significantly smaller but is stable across the frequency range. The capacitance difference between dry skin and hydrated skin for the G50W50, G100W100, and G200W200 sensors with and without encapsulation layer was also plotted in Fig. 7(g). This shows that, the G50W50 configuration is the most sensitive when either encapsulated or non-encapsulated. In contrast, G200W200, with its larger gap and width, produces lower capacitance difference between dry and hydrated skin contacting, which leads to lower sensitivity.

To further explore the impact of EVOH encapsulation layer thickness on skin sensing sensitivity, a precise spray coating method was employed to create thinner layers on G100W100 sensors. EVOH layers with thicknesses of 4  $\mu\text{m}$ , 8  $\mu\text{m}$ , and 10  $\mu\text{m}$  were fabricated. The capacitance differences between dry and hydrated skin in contact with these varying thicknesses are presented in Fig. 7(h). The decreasing capacitance difference with increasing layer thickness indicates that a thicker encapsulation layer leads to reduced sensitivity and therefore thinner layers are preferred. This result is consistent with the simulation results presented in Table 2.

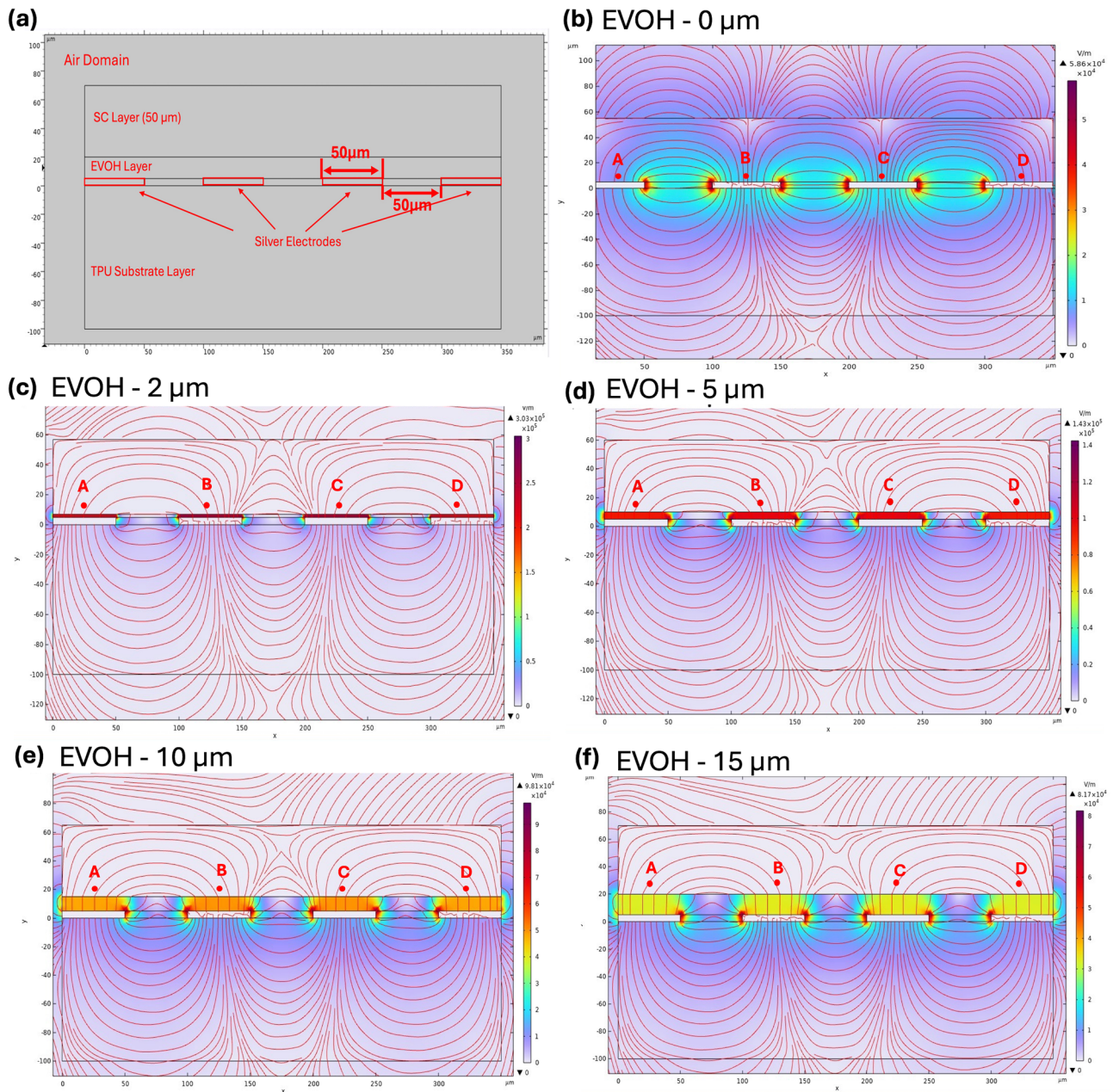


**Fig. 4 | Simulation of encapsulation layer thickness effects on IDC sensor performance in COMSOL Multiphysics. 6.1. a** 2D model of encapsulated ROP IDC Sensor with finger width of  $50\ \mu\text{m}$  and fingers gap of  $50\ \mu\text{m}$  build in COMSOL

Multiphysics. **b–f** Surface electric field strength (V/m) and generated electric field lines distribution of an IDC Sensor with EVOH encapsulation layer thicknesses of  $0\ \mu\text{m}$ ,  $2\ \mu\text{m}$ ,  $5\ \mu\text{m}$ ,  $10\ \mu\text{m}$ , and  $15\ \mu\text{m}$ .

**Table 2 | Electric field strength at four points in the SC skin layer for different EVOH thicknesses**

EVOH Layer Thickness ( $\mu\text{m}$ )	Electric Field Strength (V/m)			
	A	B	C	D
0	6566.2	10483	10465	6092.9
2	664.54	673.00	664.45	664.85
5	296.46	290.39	281.84	285.99
10	152.96	144.18	146.99	147.87
15	103.95	98.071	100.24	101.22

**Clinical Case Study on an AD Patient**

Before proceeding to future clinical patient testing, biocompatibility was assessed by reference to in vitro cytotoxicity testing—the extract and direct contact methods defined in ISO 10993-5:2009<sup>45</sup>—to detect any cell damage

or death upon material exposure. All materials in the laminated sensor stack have demonstrated compatibility with skin-contact applications. Under these assays, conductive silver nanoparticle inks—widely used in wearable electronics—have likewise passed ISO 10993-5 testing, showing >90% cell viability in L929 fibroblast assays, indicating minimal cytotoxic risk<sup>46</sup>. Starch–EVOH composite films (SEVA-C) exhibited >90% viability in human osteosarcoma (HOS) cell cultures, confirming negligible cytotoxicity of the encapsulation layer<sup>47</sup>. Additionally, EVOH copolymers (e.g., Onyx<sup>®</sup> liquid embolic agents) have been applied in vivo with no reported tissue irritation, demonstrating their non-irritating, biocompatible properties<sup>48</sup>. Finally, TPU are widely used in skin-contact medical devices (e.g., catheters, wound dressings) and have demonstrated excellent biocompatibility per ISO 10993 testing protocols<sup>49</sup>. Together, these data support the biocompatibility and non-irritating nature of the entire sensor when attached onto sensitive or AD-affected skin.

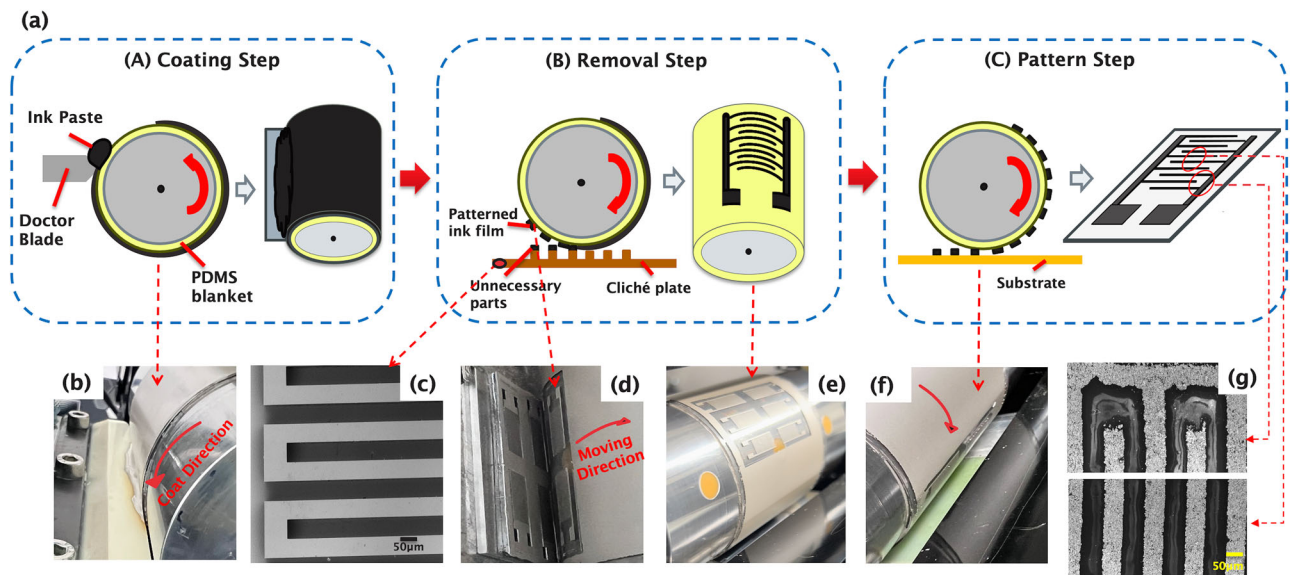


**Fig. 5 | IDC sensor fabrication processes with reverse-offset printing.** **a** Schematic diagrams of the whole ROP printing process which contains the three steps shown. **b** PDMS blanket on the roller fully coated with silver ink. **c** SEM photo of the etched silicon cliché. **d** Roller rolling across a cliché plate. **e** Desired IDC pattern remaining on the roller. **f** Transferring inks from the roller to the TPU substrate. **g** SEM photos of sections of the printed IDC electrodes (light area is printed silver, dark area is the substrate).

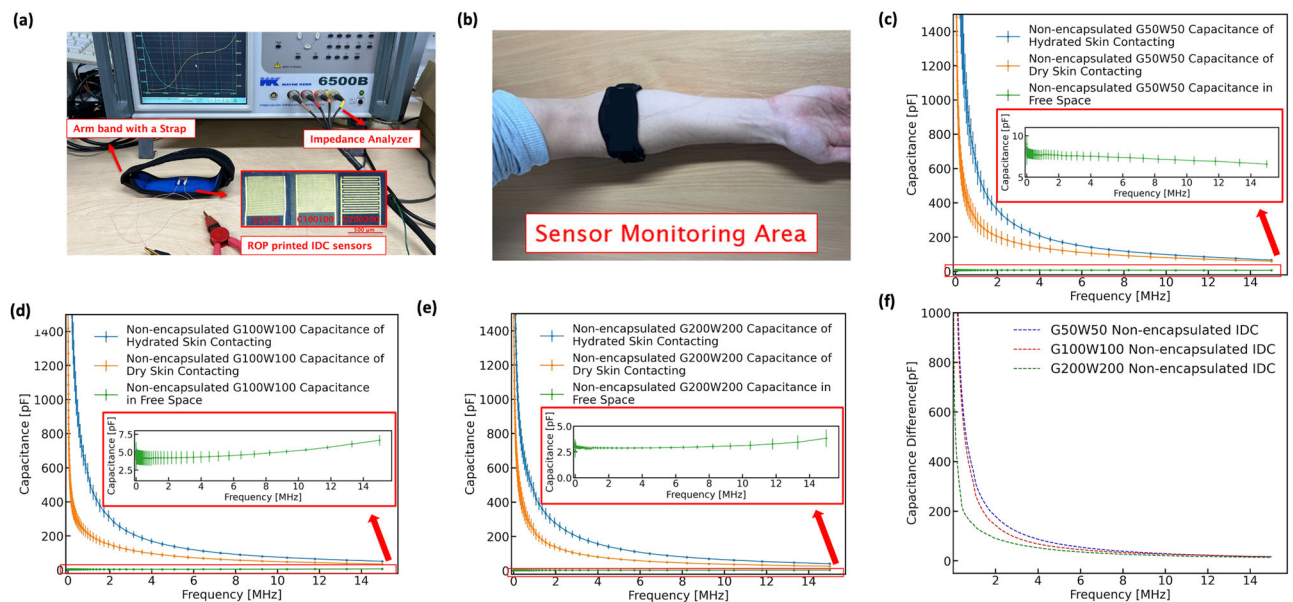


**Fig. 6 | IDC sensor testing.** **a** Impedance analyzer and sensor set up for testing. **b** Sensor location on the forearm of the person being tested. **c** Capacitance of sensors measured in free space and in contact with dry and hydrated skin: **c** G50W50 sensor; **d** G100W100 sensor; **e** G200W200 sensor. **f** Capacitance difference between the dry and hydrated skin tests vs. frequency for G50W50, G100W100 and G200W200 IDC sensors.

To evaluate the clinical efficacy of the ROP-fabricated encapsulated IDC sensors, capacitance measurements were performed on an AD patient under ethical approval (NRES 330915) with informed consent. Figure 8(a) illustrates how the sensor, integrated with a capacitance-to-digital converter for measurement, can be attached to a patient’s forearm. A dermatologist identified two areas on the patient’s right volar forearm: one with active lesions and one without visible symptoms (non-lesion). The encapsulated G50W50 sensor were placed on each site for 30 seconds to capture continuous readings. As shown in Fig. 8(b), the G50W50 sensor exhibited a mean capacitance difference of  $4.84 \pm 0.25$  pF (non-lesion:  $50.13 \pm 0.87$  pF vs. lesion:  $45.29 \pm 0.73$  pF), confirming its sensitivity to localized pathological

changes in AD. Since direct measurement of skin hydration is not feasible, two clinically validated instruments were employed as hydration proxies on lesional versus non-lesional skin. First, a dielectric-based Corneometer® (Courage+Khazaka GmbH, Cologne, Germany) measured an average hydration index of 9.97 AU on lesional skin compared to 12.93 AU on non-lesional skin (mean of 10 readings each). Second, a Tewameter® (Courage+Khazaka GmbH, Cologne, Germany) quantified transepidermal water loss (TEWL), recording  $21.29$  g/m<sup>2</sup>/h on lesional skin versus  $14.10$  g/m<sup>2</sup>/h on non-lesional skin, with higher TEWL values indicating increased dehydration. Consistent with these clinical hydration differences, the ROP-printed IDC sensors recorded larger capacitance difference on lesional skin versus

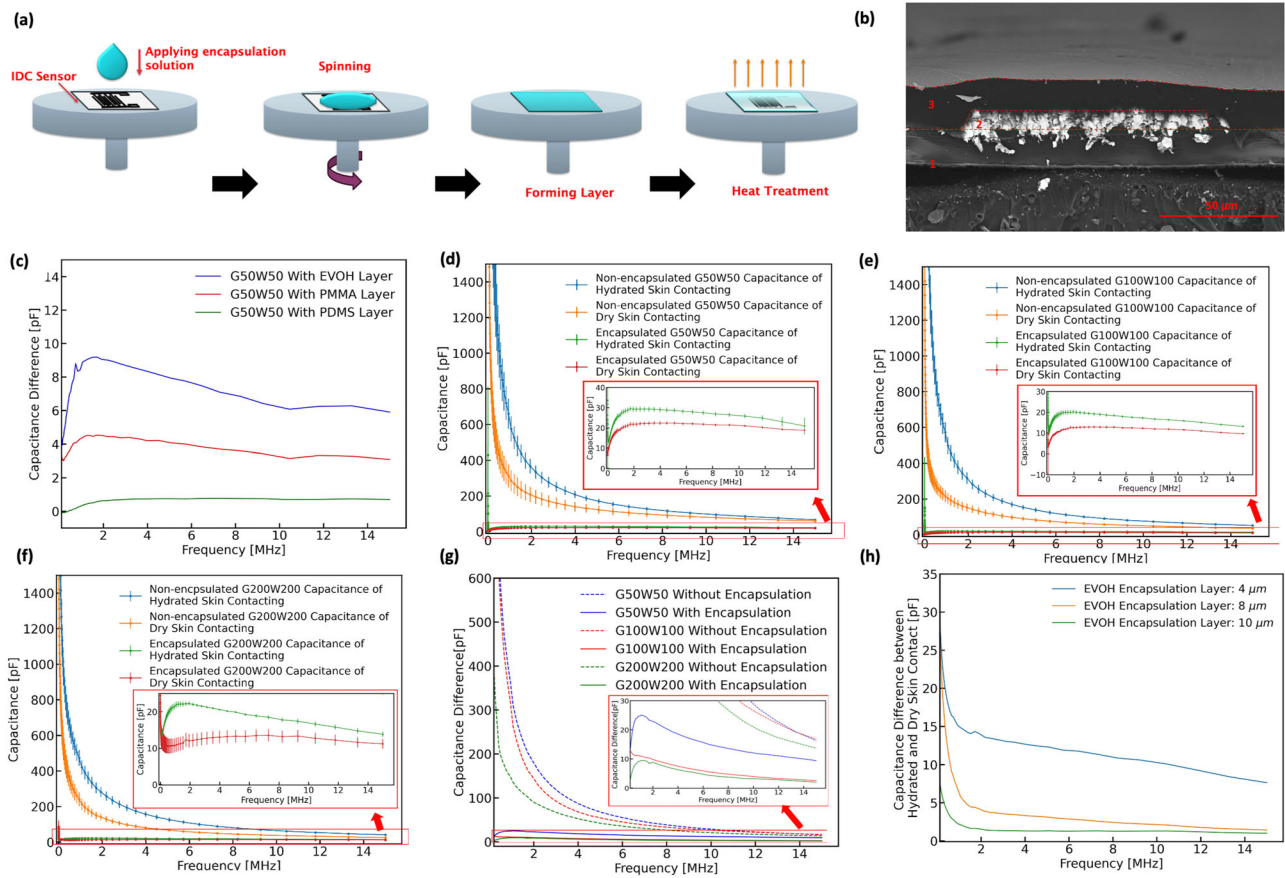
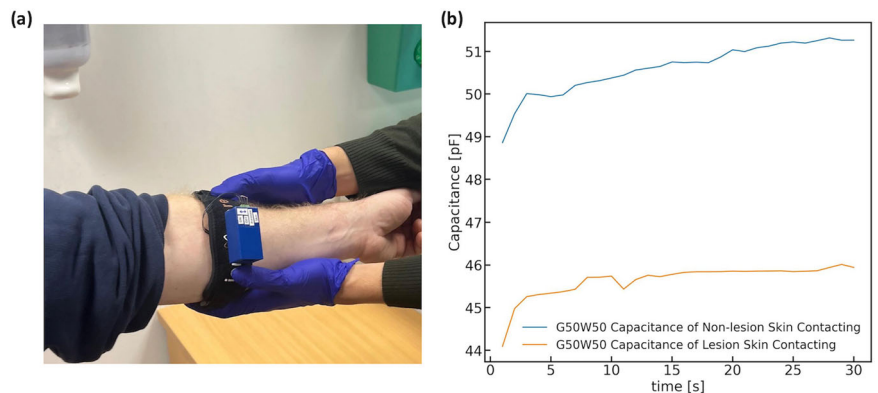


**Fig. 7 | IDC sensors with EVOH encapsulation layer added testing.** **a** Schematic diagrams of the whole encapsulation layer spin coating process. **b** SEM photo of the cross-section structure of G100W100 IDC sensor which includes TPU substrate (1), silver electrode (2) and EVOH encapsulation layer (3). **c** Capacitance difference measured from hydrated and dry skin vs. frequency for G50W50 IDC sensor with different encapsulation layers (EVOH, PMMA, PDMS). Capacitance vs. Frequency results with hydrated and dry skin contact with and without 15  $\mu\text{m}$  EVOH encapsulation layer thickness of **d** G50W50 IDC sensor (**e**) G100W100 IDC sensor and **f** G200W200 IDC sensor. **g** Capacitance difference of the EVOH-encapsulated IDC sensor with various sizes between dry and hydrated skin contact, with and without the encapsulation layer. **h** Effect of EVOH encapsulation layer thickness on the capacitance difference between dry and hydrated skin contact across frequency.

**Fig. 8 | Capacitance measurements on an AD patient with encapsulated G50W50 IDC sensors.** **a** Illustrative representation of sensor placement on forearm for clinical patient testing. **b** Time-dependent capacitance profiles of the sensor across lesioned and non-lesioned skin.



non-lesional skin, demonstrating sensitivity to the same hydration changes. Consequently, these findings establish the capability of ROP-printed IDC sensors for real-time monitoring of disease progression and treatment efficacy.

**Discussion**

The use of ROP to fabricate flexible IDC sensors on fabrics achieves smaller feature sizes than is possible with standard screen printing and this has

enabled improved sensitivity when monitoring skin moisture loss that occurs in conditions such as atopic dermatitis. The 50  $\mu\text{m}$  line width and gap were reproducibly fabricated by ROP with consistently high yield in preliminary runs, effectively concentrating the electric field in the SC to maximize sensitivity. This method effectively uses higher silver loading (70%) inks, compared to other high-resolution printing techniques, like screen printing. While achieving similar resolutions, ROP stands out by maintaining superior electrical properties, ensuring better performance and

**Table 3 | Parameters of IDC sensor built in COMSOL Multiphysics 6.1**

Parameter	Value
Gap Distance Between Two Fingers (D)	50 $\mu\text{m}$ , 100 $\mu\text{m}$ , 200 $\mu\text{m}$
Finger Width (W)	50 $\mu\text{m}$ , 100 $\mu\text{m}$ , 200 $\mu\text{m}$
Distance Between Finger End and Contact Line (G)	100 $\mu\text{m}$
Thickness of IDC Sensor Layer ( $T_{\text{IDC}}$ )	3 $\mu\text{m}$
Thickness of Substrate ( $T_{\text{sub}}$ )	160 $\mu\text{m}$
Thickness of Stratum Corneum (SC) skin Layer ( $T_{\text{SC}}$ )	50 $\mu\text{m}$
Contact Pad Area	200 $\mu\text{m}$ × 200 $\mu\text{m}$

efficiency in applications. However, the sensors do require encapsulation, and this significantly reduces sensitivity. EVOH was found to be the most suitable encapsulant and this encapsulating layer should be as thin as possible to minimise the reduction in sensitivity. Thinner encapsulation also improves sensor flexibility but could reduce the level of mechanical protection provided and hence there is a potential trade-off between sensor longevity and sensitivity that will be explored in future investigations. The experimental results show very good agreement with the COMSOL simulations indicating the suitability of numerical simulations to reliably predict sensor performance. The encapsulated IDC sensors are very well suited for monitoring AD and the compatibility with textiles presents a convenient and user-friendly implementation that enables long-term remote patient monitoring and quantification of the severity of the condition and the impact of treatments. Clinical testing on an AD patient further confirmed the G50W50 sensor's capacity to differentiate lesioned and non-lesioned skin within the same individual, underscoring its utility in personalized dermatological care. A comprehensive yield analysis involving expanded sample sets and statistical evaluation will be conducted in subsequent studies to formally quantify ROP's fabrication consistency for fine features.

## Methods

### IDC Sensor Simulation Model Built in COMSOL Multiphysics 6.1

The specific parameters of the IDC sensor model built in COMSOL Multiphysics 6.1 are shown in Table 3.

### Fabrication of ROP IDC Sensors

The IDC sensors were fabricated with a bespoke ROP printer described previously (as shown in Fig. 9)<sup>39</sup>. This enabled designs with a minimum resolution of 50 microns were successfully printed on a thermoplastic polyurethane (TPU) film attached to removable polyethylene terephthalate (PET) paper (Policrom Screens, Carvico, Italy) using Smart Fabric Inks Ltd: Fabinks TC-C4001 silver conductor paste with viscosity of 4300 cP. The resolution achieved is constrained by the features present on the cliché. The silicon cliché plates used for creating patterns were fabricated on a 525  $\mu\text{m}$  thick silicon wafer using photolithography and deep reactive ion etching (DRIE) processes with 100  $\mu\text{m}$  etch depth and 1  $\mu\text{m}$  thick silicon-dioxide mask on top of the wafer. The fabrication process involved several critical etching steps, starting with the deposition of a 1  $\mu\text{m}$  thick  $\text{SiO}_2$  hard mask using plasma-enhanced chemical vapor deposition (PECVD). Optical lithography was then applied with a 6.2  $\mu\text{m}$  thick AZ2070 resist layer. The  $\text{SiO}_2$  hard mask was etched using an inductively coupled plasma (ICP) tool with a power setting of 1500 W for the ICP and 100 W for the RF, at a temperature of 5 °C. The etch process took 6 min and 30 sec. After etching the mask, a 20-min  $\text{O}_2$  plasma ash was used to remove any remaining photoresist. DRIE was then performed using the Bosch process which achieved a depth of 107  $\mu\text{m}$  from 15 min etch time. After DRIE, S1813 resist was spun at 1000 rpm to cover the deep trenches, preparing the wafer for dicing. The dicing process, conducted using the dicing saw, cut the entire wafer into pieces corresponding to different designs and applications. Following dicing, the chips were cleaned with acetone and isopropyl alcohol

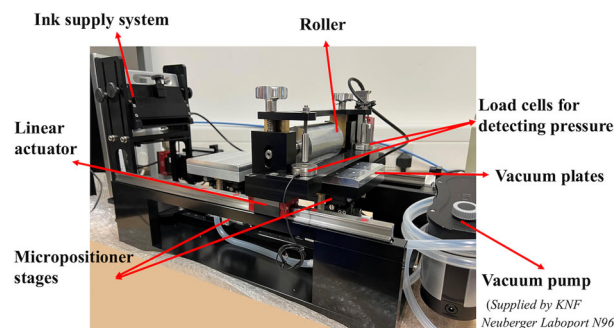


**Fig. 9 |** A bespoke reverse offset printer developed at the University of Southampton.

(IPA) to remove any remaining resist and debris. Finally, a hydrofluoric acid (HF) cleaning step was conducted to remove the  $\text{SiO}_2$  hard mask and any particles lodged during the dicing process. Following the entire ROP process, the patterned TPU films were attached to a textile armband (Ionocore®, Wistaston, UK) using a thermal lamination process at 190 °C (Geo Knight DK20 hot press), in preparation for future testing.

### Fabrication of Encapsulation Layers on IDC Sensors

**EVOH Layer Preparation.** 1 g of Poly (vinyl alcohol-co-ethylene) (EVOH) (Sigma Aldrich Chemical Company, USA) was added into 10 mL of a solvent mixture of 70 vol% IPA and 30 vol% water, and the mixture was stirred at 50 rpm at a temperature of 120 °C until the mixture turns into transparent solution. The EVOH solution was spin-coated onto the G50W50, G100W100, and G200W200 IDC sensors at 1500 rpm for 120 s. The sensors were left at room temperature for 10 min to remove the solvent gradually and then placed on a hot plate for curing at 110 °C for 30 min to form solidified EVOH film, whose average thickness was around  $15 \pm 0.05 \mu\text{m}$ . To achieve a uniform EVOH film with thicknesses of less than 10  $\mu\text{m}$ , spray coating was employed as an alternative to spin coating. A 100 mg/mL solution of EVOH in dimethyl sulfoxide (DMSO) was prepared and sprayed using an airbrush with a nozzle diameter of 300  $\mu\text{m}$  and operating at a pressure of 30 kPa. The needle cap remained positioned 10 cm from the sensor surface, continuously spraying for 2 sec per pass, resulting in the deposition of approximately 2  $\mu\text{m}$  of material with each spray. The thickness of the coated film was adjusted by applying multiple layers, with each subsequent layer added after the previous one had dried. In this way, EVOH layers with thicknesses of 4  $\mu\text{m}$ , 8  $\mu\text{m}$ , and 10  $\mu\text{m}$  were fabricated.

**PMMA Layer Preparation.** 1 g of Poly (methyl methacrylate) (PMMA) (Sigma Aldrich Chemical Company, USA) was added to 10 mL of Iso-amyl Acetate ( $\geq 97\%$ , Sigma Aldrich Chemical Company, USA) solvent and the mixture was stirred at 50 rpm for 3 h at a temperature of 70 °C. The PMMA solution was centrifuged at 4500 rpm for 15 min at room temperature to eliminate the bubbles inside. The mixture was spin-coated onto G50W50, G100W100, and G200W200 IDC sensors at 1000 rpm for 120 s. The sensors were then placed on a hot plate for a soft bake at 60 °C for 10 min followed by curing at 110 °C for 30 min to form a solidified PMMA film with average thickness around  $15 \pm 0.5 \mu\text{m}$ .

**PDMS Layer Preparation.** Poly(dimethylsiloxane) (PDMS, Sylgard 184, Dow Corning) was prepared by mixing the prepolymer with a cross-linker evenly in a weight ratio of 10:1 and left in a vacuum oven for 30 min to eliminate the bubbles in liquid PDMS. The liquid PDMS was spin-coated onto G50W50, G100W100, and G200W200 IDC sensors at 2000 rpm for 120 s. The sensors were then placed on a hot plate for a soft bake at 60 °C for 10 min followed by annealing at 110 °C for 30 minutes to form solidified PDMS film, whose average thickness was around  $13.7 \pm 0.5 \mu\text{m}$ .

## IDC Sensor Testing Process

Capacitance measurements in the lab were performed using a Wayne Kerr 6500b Impedance Analyzer using a frequency sweep from 100 Hz to 15 MHz. Measurements of pure and encapsulated IDC sensors were taken from the dry skin of a subject with AD, both before and 15 minutes after the application of a humectant cream to increase hydration levels. For each skin condition, the sensor was tested once and then removed from the skin. This cycle was repeated three times at 1-minute intervals.

For clinical validation, measurements were additionally conducted on an AD patient with dermatologist-confirmed lesions. Sensors were applied to both lesioned and non-lesioned forearm sites, and continuous readings were recorded for 30 sec. Ethical approval (NRES 330915) and informed consent were obtained. The capacitance measurement system consists of an FDC2214 capacitance-to-digital converter (Texas Instruments, USA) paired with a Xiao nRF52840 microcontroller unit (Seeed Studio, China). The system operates at 1 MHz and is housed in a compact enclosure, which is secured to the backside of the armband using Velcro tape. The armband includes a cushion to maintain consistent pressure and contact with the skin. The system utilizes an external LC tank circuit oscillating at a pre-defined frequency, determined by manually soldering discrete inductor and capacitor components (47 pF and 470  $\mu$ H in this case). When an unknown capacitance is introduced to the LC tank, the resonance frequency shifts, and the FDC2214 detects this change to compute the unknown capacitance. This hardware is an updated version of the system described in the work of Todorov, et al.<sup>50</sup>

## Morphological and Electrical Characterization

The structure and surface morphology of silicon cliché plates and ROP printed IDC sensors were inspected using a Phenom ProX Desktop Scanning Electron Microscopy (SEM) from ThermoFisher.

## Data Availability

Data is provided within the manuscript or supplementary information files.

Received: 7 April 2025; Accepted: 9 July 2025;

Published online: 02 August 2025

## References

- Huang, Z. et al. Recent advances in skin-like wearable sensors: Sensor design, health monitoring, and intelligent auxiliary. *Sens. Diagn.* **1**, 686–708 (2022).
- Luo, Y. et al. Learning human–environment interactions using conformal tactile textiles. *Nat. Electron.* **4**, 193–201 (2021).
- Lou, Z., Wang, L. & Shen, G. Recent advances in smart wearable sensing systems. *Adv. Mater. Technol.* **3**, 1–17 (2018).
- Mazzocchi, T., Diodato, A., Ciuti, G., De Micheli, D. M. & Menciassi, A. Smart sensorized polymeric skin for safe robot collision and environmental interaction. In *2015 IEEE/RSJ International Conference on Intelligent Robots and Systems (IROS)*, 837–843, (2015).
- Jang, M., Kim, H.-D., Koo, H.-J. & So, J.-H. Textile-based wearable sensor for skin hydration monitoring. *Sensors* **22**, <https://doi.org/10.3390/s22186985> (2022).
- Madhvapathy, S. R. et al. Reliable, low-cost, fully integrated hydration sensors for monitoring and diagnosis of inflammatory skin diseases in any environment. *Sci. Adv.* **6**, 1–12 (2020).
- Li, F., Xue, H., Lin, X., Zhao, H. & Zhang, T. Wearable temperature sensor with high resolution for skin temperature monitoring. *ACS Appl. Mater. Interfaces* **14**, 43844–43852 (2022).
- Trung, T. Q. et al. A stretchable strain-insensitive temperature sensor based on free-standing elastomeric composite fibers for on-body monitoring of skin temperature. *ACS Appl. Mater. Interfaces* **11**, 2317–2327 (2019).
- McLister, A., Phair, J., Cundell, J. & Davis, J. Electrochemical approaches to the development of smart bandages: a mini-review. *Electrochem. Commun.* **40**, 96–99 (2014).
- McLister, A., McHugh, J., Cundell, J. & Davis, J. New developments in smart bandage technologies for wound diagnostics. *Adv. Mater.* **28**, 5732–5737 (2016).
- Oh, Y. S. et al. Battery-free, wireless soft sensors for continuous multi-site measurements of pressure and temperature from patients at risk for pressure injuries. *Nat. Commun.* **12**, 1–16 (2021).
- Stannett, M. Membrane systems and hypercomputation. *Lect. Notes Comput. Sci. (including subseries Lect. Notes Artif. Intell. Lect. Notes Bioinformatics)* **7762 LNCS**, 78–87, (2012).
- Flohr, C., Johansson, S., Wahlgren, C.-F. & Williams, H. How atopic is atopic dermatitis?. *J. Allergy Clin. Immunol.* **114**, 150–158 (2004).
- Wang, V., Boguniewicz, J., Boguniewicz, M. & Ong, P. Y. The infectious complications of atopic dermatitis. *Ann. Allergy, Asthma Immunol.* **126**, 3–12 (2021).
- Thomsen, S. F. Atopic Dermatitis: Natural History, Diagnosis, and Treatment. *ISRN Allergy* **2014**, 1–7 (2014).
- Todorov, A. R., Torah, R., Arden-Jones, M. & Beeby, S. Fabrication of a screen-printed e-textile interdigitated capacitive sensor for measuring stratum corneum hydration. *Eng. Proc.* **52**, <https://doi.org/10.3390/engproc2023052001> (2023).
- Yilmaz, A. F. et al. Highly Stretchable textile knitted interdigital sensor for wearable technology applications. *Adv. Sens. Res.* **3**, 1–10 (2024).
- Yuan, L. et al. Flexible, anisotropic strain sensor based on interdigital capacitance for multi-direction discrimination. *Sens. Actuators A: Phys.* **359**, 114459 (2023).
- Kanaparthi, S. & Badhulika, S. Low cost, flexible and biodegradable touch sensor fabricated by solvent-free processing of graphite on cellulose paper. *Sens. Actuators B: Chem.* **242**, 857–864 (2017).
- Abdullah al Rumon, M. & Shahariar, H. Fabrication of interdigitated capacitor on fabric as tactile sensor. *Sens. Int* **2**, 100086 (2021).
- Alanen, E., Nuutinen, J., Nicklén, K., Lahtinen, T. & Mönkkönen, J. Measurement of hydration in the stratum corneum with the MoistureMeter and comparison with the Corneometer. *Ski. Res. Technol.* **10**, 32–37 (2004).
- Malnati, C., Fehr, D., Spano, F. & Bonmarin, M. Modeling stratum corneum swelling for the optimization of electrode-based skin hydration sensors. *Sensors* **21**, <https://doi.org/10.3390/s21123986> (2021).
- Ganbold, E. et al. Highly Sensitive Interdigitated Capacitive Humidity Sensors Based on Sponge-Like Nanoporous PVDF/LiCl Composite for Real-Time Monitoring. *ACS Appl. Mater. Interfaces* **15**, 4559–4568 (2023).
- Sapsanis, C. et al. A nafion coated capacitive humidity sensor on a flexible PET substrate. *Midwest Symp. on Circuits Syst.* **0**, <https://doi.org/10.1109/MWSCAS.2016.7870020> (2016).
- Kim, C. U. et al. Numerical analysis on effective electric field penetration depth for interdigital impedance sensor. *J. Phys.: Conf. Ser.* **418**, 0–9 (2013).
- Huang, Y., Zhan, Z. & Bowler, N. Optimization of the coplanar interdigital capacitive sensor. *AIP Conf. Proc.* **1806**, <https://doi.org/10.1063/1.4974695> (2017).
- Ranjan, P. & Chowdhury, A. Comparative Study of IDC Sensor's Geometrical Effect, Performance, and Frequency Behaviour with Water Level Detection. *Instrum. Exp. Tech.* **66**, 315–323 (2023).
- Mizuguchi, J. et al. Fringing field capacitive sensor for measuring soil water content: Design, manufacture, and testing. *IEEE Trans. Instrum. Meas.* **64**, 212–220 (2015).
- Chon-ung Kim, C. et al. Numerical analysis on effective electric field penetration depth for interdigital impedance sensor. *J. Phys.: Conf. Ser.* **418**, 012020 (2013).
- Bonnassieux, Y., et al. The 2021 flexible and printed electronics roadmap. *Flex. Print. Electron.* **6**, abf986 (2021).
- Martins, P. et al. Advances in Printing and Electronics: From Engagement to Commitment. *Adv. Funct. Mater.* **33**, 2213744 (2023).

32. Yang, F., Huang, Y., Li, Y. & Li, Y. Large-area flexible organic solar cells. *npj Flex. Electron.* **5**, 1–12 (2021).
33. Park, J. W., Kang, B. H. & Kim, H. J. A Review of Low-Temperature Solution-Processed Metal Oxide Thin-Film Transistors for Flexible Electronics. *Adv. Funct. Mater.* **30**, 1–40 (2020).
34. Zabhipour, M. et al. High yield manufacturing of fully screen-printed organic electrochemical transistors. *npj Flex. Electron.* **4**, 1–8 (2020).
35. Gugliandolo, G. et al. Inkjet-Printed Interdigitated Capacitors for Sensing Applications: Temperature-Dependent Electrical Characterization at Cryogenic Temperatures down to 20 K. *Instruments* **7**, <https://doi.org/10.3390/instruments7030020> (2023).
36. Bezel, I. V. I. & Applications, D. Nanoparticle-Based Flexible Capacitive Sensor for Automotive. (2023).
37. Choi, Y. M., Lee, E. S., Lee, T. M. & Kim, K. Y. Optimization of a reverse-offset printing process and its application to a metal mesh touch screen sensor. *Microelectron. Eng.* **134**, 1–6 (2015).
38. Søndergaard, R. R., Hösel, M. & Krebs, F. C. Roll-to-Roll fabrication of large area functional organic materials. *J. Polym. Sci. Part B: Polym. Phys.* **51**, 16–34 (2013).
39. Dai, H., Torah, R. & Beeby, S. Reverse-Offset Printing for Fabricating E-Textiles. *Eng. Proc.* **52**, <https://doi.org/10.3390/engproc2023052014> (2023).
40. Gabriel, S., Lau, R. W. & Gabriel, C. The dielectric properties of biological tissues: III. Parametric models for the dielectric spectrum of tissues. *Phys. Med. Biol.* **41**, 2271–2293 (1996).
41. McDonald, J. C. & Whitesides, G. M. Poly(dimethylsiloxane) as a material for fabricating microfluidic devices. *Acc. Chem. Res.* **35**, 491–499 (2002).
42. Barkoula, N. M., Alcock, B., Cabrera, N. O. & Peijs, T. Flame-Retardancy Properties of Intumescent Ammonium Poly(Phosphate) and Mineral Filler Magnesium Hydroxide in Combination with Graphene. *Polym. Polym. Compos.* **16**, 101–113 (2008).
43. Ali, U., Karim, K. J. B. A. & Buang, N. A. A Review of the Properties and Applications of Poly (Methyl Methacrylate) (PMMA). *Polym. Rev.* **55**, 678–705 (2015).
44. Reddy, A. S. et al. Printed capacitive based humidity sensors on flexible substrates. *Sens. Lett.* **9**, 869–871 (2011).
45. ISO. Biological evaluation of medical devices—Part 5: Tests for in vitro cytotoxicity. ISO Standard 10993-5:2009. *Int. Org. for Standardization, Geneva, Switzerland*, (2009).
46. Składanowski, M., Golińska, P., Rudnicka, K., Dahm, H. & Rai, M. Evaluation of cytotoxicity, immune compatibility and antibacterial activity of biogenic silver nanoparticles. *Med. Microbiol. Immunol.* **205**, 603–613 (2016).
47. Gomes, M. E. et al. Cytocompatibility and response of osteoblastic-like cells to starch-based polymers: effect of several additives and processing conditions. *Biomaterials* **22**, 1911–1917 (2001).
48. Minici, R. et al. Endovascular treatment of visceral artery pseudoaneurysms with ethylene-vinyl alcohol (EVOH) copolymer-based non-adhesive liquid embolic agents (NALEAs). *Medicina* **59**, 1606 (2023).
49. Med-Tech Insights, TPU—Your Flexible Friend. Med-Tech Insights, 21 Sep. 2021. [Online]. Available: <https://med-techinsights.com/2021/09/21/tpu-your-flexible-friend> (Accessed: 12 May 2025).
50. Todorov, A. R., Dai, H., Torah, R., Arden-Jones, M. & Beeby, S. Wearable interdigital e-textile sensor for monitoring atopic dermatitis in patients. *Manuscript in preparation*.
51. Au, C.-Y. et al. A Sensorised Glove to Detect Scratching for Patients with Atopic Dermatitis. *Sensors* **23**, 9782 (2023).
52. J.-E. Kim, J. Lee, M. Bessho and K. Sakamura. Field Trial of a Wearable Itch Monitoring System for the Self-Management of Atopic Dermatitis. *2021 IEEE International Conference on Systems, Man, and Cybernetics (SMC), Melbourne, Australia*, pp. 2457–2463, (2021).

## Acknowledgements

The work of SB was supported by the Royal Academy of Engineering under the Chairs in Emerging Technologies Scheme. I also thank Dr. Anushka Gangnaik and Dr. Liam Boodhoo for helping with the cliché plate fabrication.

## Author contributions

H.D. carried out the printer design, experiment implementation, sensor testing and wrote the manuscript draft. A.R.T. carried out the cliché design, clinical sensor testing and capacitance measurement system manufacture. S.Y. contributed to the selection and preparation of encapsulation materials. R.T. contributed to the selection of conductive and substrate materials, printer development and supervision for the research, M.A.-J. provided supervision for the research work. S.B. provided supervision for the research work and edited the manuscript draft. All authors reviewed the manuscript.

## Ethical approval

The study was done in conjunction with the NOMAD study, ethics approval: NRES 330915.

## Competing interests

The authors declare no competing interests.

## Additional information

**Supplementary information** The online version contains supplementary material available at <https://doi.org/10.1038/s41528-025-00456-x>.

**Correspondence** and requests for materials should be addressed to Huanghao Dai or Steve Beeby.

**Reprints and permissions information** is available at <http://www.nature.com/reprints>

**Publisher's note** Springer Nature remains neutral with regard to jurisdictional claims in published maps and institutional affiliations.

**Open Access** This article is licensed under a Creative Commons Attribution 4.0 International License, which permits use, sharing, adaptation, distribution and reproduction in any medium or format, as long as you give appropriate credit to the original author(s) and the source, provide a link to the Creative Commons licence, and indicate if changes were made. The images or other third party material in this article are included in the article's Creative Commons licence, unless indicated otherwise in a credit line to the material. If material is not included in the article's Creative Commons licence and your intended use is not permitted by statutory regulation or exceeds the permitted use, you will need to obtain permission directly from the copyright holder. To view a copy of this licence, visit <http://creativecommons.org/licenses/by/4.0/>.

© The Author(s) 2025